Cancer Chemother Pharmacol (2006) 58: 607–617
DOI 10.1007/s00280-006-0208-7

ORIGINAL ARTICLE

Ruediger E. Port · Christian Schuster
Christa R. Port · Peter Bachert

Simultaneous sustained release of fludarabine monophosphate and Gd-DTPA from an interstitial liposome depot in rats: potential for indirect monitoring of drug release by magnetic resonance imaging

Received: 18 October 2005 / Accepted: 7 February 2006 / Published online: 28 February 2006

Abstract *Introduction*: Cytostatic depot preparations are interstitially administered for local chemotherapy and prevention of tumor recurrence. It would be of interest to monitor in patients as to when, to what extent, and exactly where, the drug is actually released. Liposomes containing a hydrophilic cytostatic and a hydrophilic contrast agent might be expected to release both agents simultaneously. If so, then drug release could be indirectly followed by monitoring contrast enhancement at the injection site. *Methods*: Multivesicular liposomes containing the antimetabolite fludarabine monophosphate and the magnetic resonance imaging (MRI) contrast agent Gd-DTPA were subcutaneously injected in rats and both agents were monitored at the injection site for 6 weeks by ^{19}F nuclear magnetic resonance spectroscopy (MRS) in vivo and contrast-enhanced ^{1}H MRI (T_{1w} 3D FLASH), respectively, in a 1.5-T whole-body tomograph. The MRS and MRI data were analyzed simultaneously by pharmacokinetic modeling using NONMEM. *Results*: During an initial lag time, the amount of drug at the injection site stayed constant while the contrast-enhanced depot volume expanded beyond the volume injected. Drug amount and depot volume then decreased in parallel. Lag time and elimination half-life were 9 and 6 days, respectively, in three animals, and were about 50% shorter in another animal where the depot split into sub-depots. *Conclusion*: The preliminary data in rats suggest that simultaneous release of a hydrophilic cytostatic and a hydrophilic contrast agent from an interstitial depot can be achieved by encapsulation in liposomes. Thus, there seems to be a potential for indirect drug monitoring through imaging.

Keywords Fludarabine monophosphate · Fluorine MR spectroscopy · Liposomes · Gd-DTPA · MR imaging

R. E. Port · C. R. Port
Unit Pharmacology of Cancer Treatment,
German Cancer Research Center,
69009, Heidelberg, Germany

C. Schuster · P. Bachert (✉)
Department of Medical Physics in Radiology,
German Cancer Research Center,
69009, Heidelberg, Germany
E-mail: p.bachert@dkfz.de

Introduction

When sustained-release preparations of cytostatics are interstitially administered for local treatment or prevention of recurrence of malignant tumors [8, 14, 21, 23] it would be of interest to monitor when, to what extent, and exactly where, the drug is actually released. Especially when the therapeutic result in an individual patient is disappointing, this information would help assess whether failure may have been due to inadequate drug delivery, or whether the drug itself is possibly ineffective in this case.

Little is known about the kinetics of drug release in this setting as drug concentrations in plasma are low or undetectable [5, 11]. The local distribution of drug solutions after interstitial infusion can be visualized by mixing with a contrast agent for magnetic resonance imaging (MRI) [19, 42]. The location and persistence of drug-carrying solid materials can also be monitored by imaging, with or without radio-labeling [15] or encapsulation of contrast agents [6, 36, 37]. These images, however, may not be informative with regard to drug release because the carrier material may persist at the administration site long after the drug has been released [12, 18]. A major step forward towards local monitoring of drug release has been to encapsulate a drug-MRI contrast agent complex in thermolabile liposomes. After systemic administration in tumor-bearing mice and application of hyperthermia to the tumor, a sudden transient MRI contrast enhancement could be observed

in tumor indicating the site and the time of a one-time, triggered release of liposome contents [41].

We have looked into the possibility of indirectly monitoring the sustained release of a cytostatic from an interstitial depot. It was speculated that a hydrophilic cytostatic and a hydrophilic contrast agent, when encapsulated in liposomes, would both be released only upon disintegration of the liposomal membranes so that, after interstitial injection, the contrast agent at the injection site could serve as an indirect indicator of the amount of drug remaining to be released. To explore the chances of this concept, the hydrophilic antimetabolite fludarabine monophosphate (FLAMP) and the even more hydrophilic MRI contrast agent Gd-DTPA (gadolinium diethyl triamino pentaacetic acid, gadopentetate) were encapsulated in multivesicular liposomes and, after subcutaneous injection in rats, both agents were monitored at the injection site by repeated ^{19}F nuclear magnetic resonance spectroscopy (MRS) in vivo and ^{1}H MRI.

Methods

Animals and setup of experiments

Experiments were carried out in accordance with the German law for animal protection and were approved by the local district government (Regierungspraesidium Karlsruhe 35-9185.81/33-99). Male Wistar rats (Charles River Wiga, Sulzfeld, Germany), 3–4 months old at the beginning of the experiments, were kept in a micro-isolator under climatized conditions, with access to standard food pellets (Altromin™) and water ad libitum. The weights of the animals increased from 350–420 g at the beginning of the experiments to 430–540 g at the end of the observation period after 4–6 weeks. Each of the three rats received a subcutaneous injection of 1 ml of a semi-solid, gel-like liposome suspension containing FLAMP and Gd-DTPA (preparation see below) in the right flank. In one other rat, the subcutaneous injection was set between the right hip and the root of the tail, in order to better prevent imaging artefacts from breathing motion. ^{19}F MRS and ^{1}H MRI examinations (see below) were carried out one to four times during the first week after the injection, and then at approximately weekly intervals until 4.5–6 weeks after the injection (cf. Fig. 2). Animals were kept in light narcosis during the MR measurements by inhalation of an O_2/N_2O mixture (20/80%, v/v) containing isoflurane, 2% for induction (ca. 30 min) and 1–1.5% for maintenance, through a standard infusion tubing fitted with the open part of a 10 ml injection syringe.

In a control animal, 1 ml of an isotonic solution containing 34 µmol FLAMP and 0.21 µmol Gd-DTPA in phosphate buffered saline was injected subcutaneously in the flank, followed immediately and after 6 and 24 h by the same MRS and MRI examinations as in the experiments where liposomes were injected.

Liposome preparation

FLAMP was obtained as a 68 mM iso-osmolar solution, pH 7.7, containing D-mannitol and sodium hydroxide, by reconstituting the (dry powder) content of Fludara™ vials (Schering AG, Berlin, Germany) with 2 ml aq. bidest. Gadopentetate was used in the form of Magnevist™ (a 0.5 M solution of the dimeglumine salt; Schering AG, Berlin, Germany). Phospholipon 90 H™ was a generous gift from Nattermann Phospholipid GmbH, Koeln, Germany; it is a mixture of hydrogenated soybean phosphatidylcholine, 95%, and lyso-phosphatidylcholine, max. 4%, with a fatty acid composition of about 85% stearic acid and 15% palmitic acid; the phase transition temperature of a 20% dispersion in water is approximately 54°C. Phosphate buffer (PBS Dulbecco's w/o Ca and Mg) was obtained from Life Technologies, Paisley, Scotland. Triton X-100 was purchased from GERBU Biotechnik GmbH, Gaiberg, Germany.

Liposomes were prepared by the freeze-and-thaw method [20]. First, multilamellar liposomes were produced by adding 200 mg Phospholipon 90 H and 1.7 µl Magnevist to 2 ml of the FLAMP solution; the dispersion was rotated for 20 min (10 rpm) and then vortexed intermittently for 30 min (2 min vortexing, 3 min interval in a waterbath at 68°C), followed by six freeze-thaw cycles: 3 min liquid nitrogen and 6 min waterbath at 68°C.

Liposomes were washed five times to remove unincorporated material by redispersing in 10 ml iso-osmolar phosphate buffer and centrifugating at 10,000*g* for 15 min. The last pellet, a semi-solid gel-like mass, was transferred to a 2 ml-syringe with a spatula for injection in rats. The amount of FLAMP in the injection volume of 1 ml was 41–52 µmol (15–19 mg, three measurements), corresponding to a trapping efficiency of 60–76% which is in accordance with reported values for impermeable solutes at the same lipid concentration (100 mg/ml) [7]. Assuming the same trapping efficiency for Gd-DTPA, the amount of Gd-DTPA in the injection volume of 1 ml was 0.25–0.32 µmol corresponding to a presumable Gd-DTPA concentration in intra-liposomal water near 0.5 mmol/l.

Drug release was determined in vitro by resuspending the last liposome pellet in an equal volume of buffer (about 2 ml), and rotating 0.5 ml samples in 2.0 ml Eppendorf vials at 10 rpm in an incubator at 37°C for up to 6 weeks. Vials were removed at approximately weekly intervals and centrifugated at 10,000*g* for 15 min, and the amounts of FLAMP were determined in pellet and supernatant. The pellet, about 0.25 ml, was dissolved in 5.0 ml Triton X-100 10% (w/v) and aq. bidest. ad 25 ml, in a 70°C waterbath. 20 µl samples of the dissolved pellet and the supernatant were analyzed by HPLC on RP-18 columns (LiChroCART™ 250-4, Merck KGaA, Darmstadt, Germany) with $NaH_2PO_4 \cdot H_2O$ (Merck KGaA), 0.02 M, as the eluent and UV detection at 265 nm. The amount of FLAMP remaining within liposomes decreased gradually to reach 74.4% of the

initial amount by 6 weeks. Total recovery of FLAMP (pellet + supernatant) was 96–102%, independent of time, showing that no degradation occurred.

Magnetic resonance methods

^{1}H MRI and ^{19}F MRS experiments were performed on a broadband 1.5-T whole-body tomograph (Magnetom Vision Plus with Helicon magnet; Siemens AG, Erlangen, Germany). A home-built volume coil (tuneable to ^{1}H and ^{19}F Larmor frequency) with a length of 14 cm and an inner diameter of 8.4 cm of the solenoid was used for both radiofrequency transmission and detection.

Animals were positioned with the liposome depot in the center of the coil. After shim (optimization of the spatial homogeneity of the magnetic field) using the tissue water ^{1}H resonance, the coil was tuned to ^{19}F frequency (59.85 MHz) for ^{19}F MRS. The frequency was then set back to ^{1}H frequency (63.63 MHz) for 3D ^{1}H MRI.

^{19}F MR spectroscopy

Fluorine-19 MR spectra were obtained without spatial localization using a one-pulse-acquire sequence with a pulse of rectangular shape and 100 μs width and a signal acquisition period of 51.2 ms (1,024 complex data points) taking into account short T_2^*. In order to maximize the signal-to-noise ratio (SNR) per unit of time in this experimental setup, a large number of excitations, NEX = 20,000, and a repetition time TR = 100 ms were used resulting in a measurement time of 33:21 min.

Postprocessing was performed with the commercial software LUISE (Siemens), available with the Magnetom Vision scanner, and consisted of zero filling to 4,096 data points and multiplying the FID by a Gaussian function for apodization (linebroadening: 30 Hz), followed by Fourier transformation, phase correction, and baseline correction. Representative spectra are shown in Figs. 1, 2. For quantification, spectra were automatically fitted assuming Gaussian line shapes and the integrals of the peaks (“MR signal intensity”) were determined.

A 2 ml sample of a 50 mM solution of trifluoroacetate (TFA) positioned inside the solenoid coil served as chemical-shift and signal-intensity reference in animal no. 1. It was replaced by a 0.5 ml sample of a 400 mM sodium fluoride solution (NaF, chemical shift relative to TFA: δ = –40.4 ppm) in animal nos. 2–4 in order to avoid interference with small amounts of TFA formed from isoflurane during narcosis (Fig. 1).

^{1}H MR imaging

A standard T_1-weighted 3D FLASH imaging protocol with fat signal suppression was used for the acquisition of ^{1}H MR images. Measurement parameters were: TR = 45 ms; echo time, TE = 11 ms; flip angle, $\alpha = 30°$; field of view, FOV = (50 mm)^2; matrix size: 128×128, resulting in-plane resolution: (0.39 mm)^2; and signal acquisition period: 15.36 ms. Fat signal suppression was achieved by means of a preceding chemical-shift-selective (CHESS) radiofrequency pulse of duration 9,782 μs and a flip angle $\alpha = 120°$.

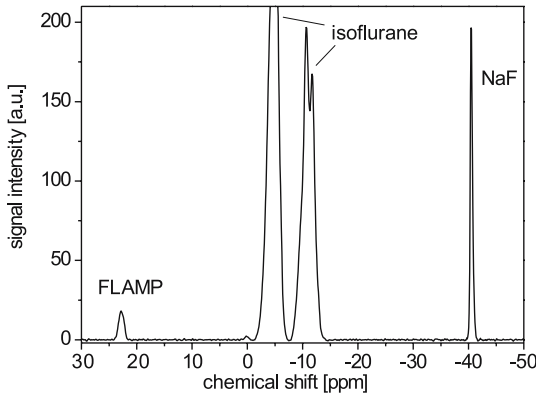

Fig. 1 In vivo 1.5-T ^{19}F MR spectrum, obtained in animal no. 3 on day 4, from 83 to 116 min after the beginning of narcosis with isoflurane. Resolved resonances with chemical shifts (δ), relative to trifluoroacetate ($\delta = 0$; small amounts formed from isoflurane during narcosis): FLAMP: $\delta = 22.9$ ppm, isoflurane: δ = –5.0, –10.7, –11.7 ppm, NaF (signal intensity reference): δ = –40.4 ppm. The SNR of the FLAMP resonance is about 20. Measurement parameters: TR = 100 ms, NEX = 20,000, measurement time = 33:21 min. Linebroadening: 30 Hz

On each examination day, axial 3D images with 2 mm slice thickness were acquired first to localize the liposome depot and to determine its spatial extension. 3D FLASH images were then acquired with a slab thickness of 32–48 mm, a fixed slice thickness of 0.4 mm and NEX = 4 resulting in a total measurement time of 31–46 min.

The 3D images with 0.4 mm slice thickness were segmented with ImageJ [32] to determine the total volume and the average signal intensity of the liposome depot. A volume of interest (VOI) containing the contrast-enhanced liposome depot and surrounding tissue was chosen for the whole 3D image stack, and the minimum signal intensity of voxels within the liposome depot was determined from a histogram of all signal intensities within this VOI. This threshold value was visually checked in all slices. All voxels with signal intensity above the threshold were counted and their total volume and average signal intensity was calculated. Calculations were repeated with two different threshold values, one 10% above and one 10% below the original one, and the standard deviation of the calculated volumes and signal intensities was used as an estimate of measurement error. The average signal intensity of the liposome depot was divided by the average signal intensity of a VOI containing nearby muscle tissue for comparisons between measurement days.

ImageJ [32] was also used to make 3D-projection images with the brightest point method (no opacity, no depth cueing).

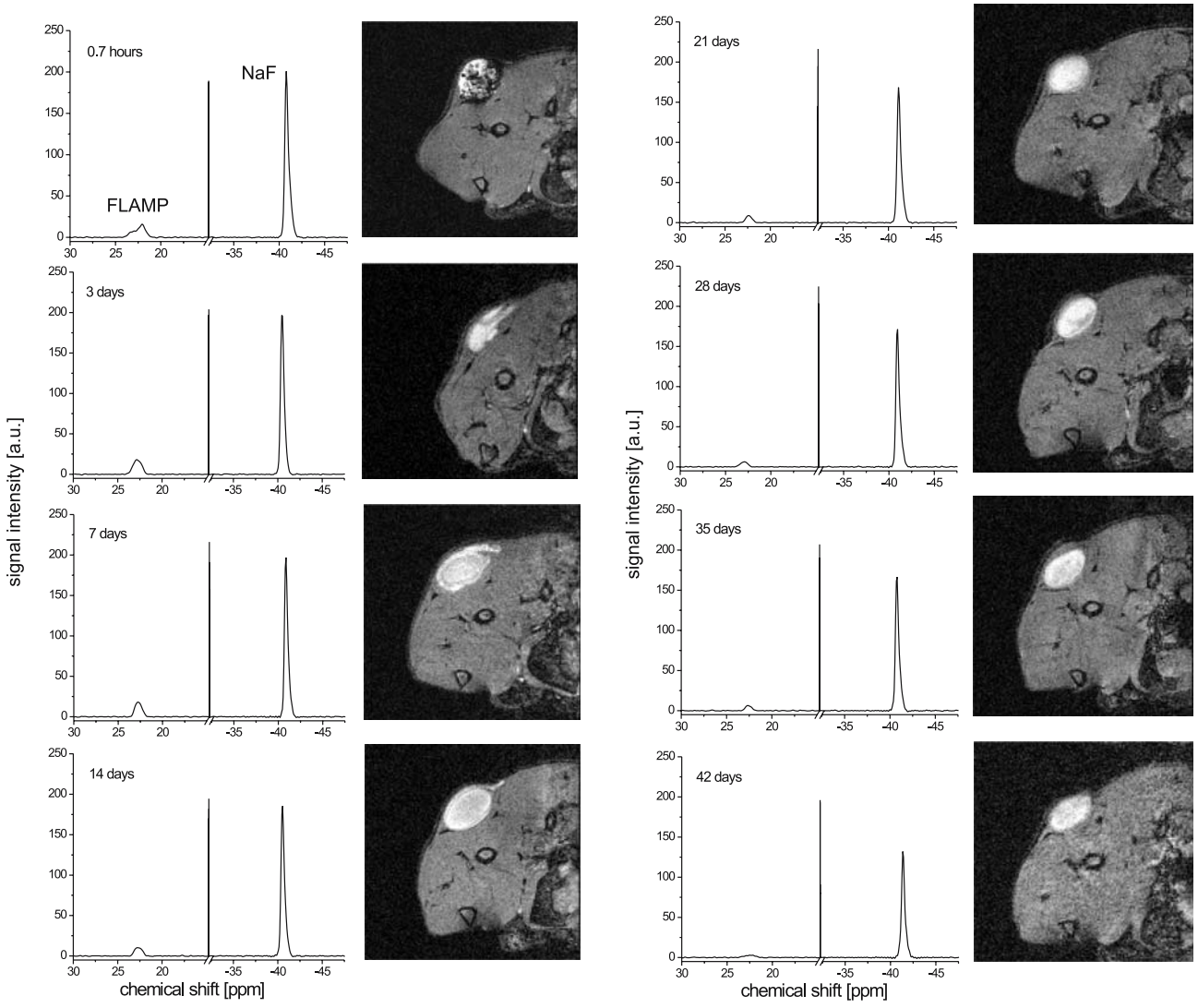

Fig. 2 In vivo 1.5-T ^{19}F MR spectra obtained 0.7 h and 3–42 days after injection of the liposome preparation, and transversal ^{1}H MR images acquired about 1 h after MRS (animal no. 3). Resolved resonances with chemical shifts: FLAMP: $\delta = 22.9$ ppm, NaF: $\delta = -40.4$ ppm. Central sections of the drug depot are shown. Measurement parameters: MRS: see Fig. 1; MRI: T_{1w} 3D FLASH with fat suppression, TR = 45 ms, TE = 11 ms, FOV = (50 mm)^2, slice thickness 0.4 mm

Pharmacokinetic analysis

The time course of the ratio of the signal intensities of FLAMP and the reference was modeled by assuming that the amount of FLAMP stays constant during a lag time (most obvious in animals 1 and 3, Fig. 5), followed by first-order elimination which may approach a plateau above zero:

$$\hat{y}(t \le t_{\mathrm{lag}}) = S_0, \tag{1}$$

$$\hat{y}(t > t_{\mathrm{lag}}) = S_0\left[\mathrm{fr} + (1 - \mathrm{fr}) \times \mathrm{e}^{-\lambda\left(t - t_{\mathrm{lag}}\right)}\right], \tag{2}$$

where $\hat{y}(t)$ is the predicted signal intensity ratio at time t, t_{lag} is lag time, S_0 is the prediction from $t = 0$ to $t = t_{\mathrm{lag}}$, fr is a fraction of the initial FLAMP amount that is apparently not touched by elimination, and λ is a first-order elimination rate constant.

The volume of contrast enhancement at the injection site was observed to increase for about a week after the injection (Fig. 5, animals 2–4) and to decrease monotonously thereafter. In the kinetic model, it was assumed to increase linearly from a fictitious minimum, V_{min}, at $t = 0$, to a maximum, V_{max}, at $t = t_{\mathrm{lag}}$, and then to decrease at the same rate as the amount of FLAMP at the injection site:

$$\hat{y}(t \le t_{\mathrm{lag}}) = V_{\mathrm{min}} + (V_{\mathrm{max}} - V_{\mathrm{min}}) \times \frac{t}{t_{\mathrm{lag}}}, \tag{3}$$

$$\hat{y}(t > t_{\mathrm{lag}}) = V_{\mathrm{max}}\left[\mathrm{fr} + (1 - \mathrm{fr}) \times \mathrm{e}^{-\lambda\left(t - t_{\mathrm{lag}}\right)}\right], \tag{4}$$

where $\hat{y}$ is the predicted volume. Note that the parameters t_{lag}, fr, and λ are common to the FLAMP and the contrast agent models. V_{min}, the extrapolated volume at time zero, is a "fictitious" volume in that it is allowed to

differ from the actually injected volume, 1 ml. It is a tool for predicting the volume at later times, much like the fictitious concentration of drugs in plasma at time zero after an intravenous bolus injection which is commonly used in modeling systemic pharmacokinetics [34].

The data of animals 1–3 were analyzed simultaneously by applying "mixed-effects modeling" [25, 27, 30, 39] which means fitting *distributions* of kinetic parameters, defined by mean and inter-individual variance parameters, rather than individual parameters. This is predicated on the assumption that the individuals studied are basically similar and vary only randomly about a common central tendency. A practical advantage of this approach is that sparse data can be utilized which would not suffice to estimate all parameters of the kinetic model when analyzing each individual's data separately. The available data were indeed "sparse" in this sense in that most measurements were 1 week or longer apart so that it would have been difficult to estimate lag times without the synopsis of three animals.

The parameter distributions were modeled by assuming:

$$P_{ki} = \overline{P_k} + \eta_{ki}, \tag{5}$$

where P_{ki} is parameter k (one of t_{lag}, fr, λ, V_{min}, V_{max}) in individual i, $\overline{P_k}$ is the mean of the distribution, and η_k varies randomly across individuals with mean zero and variance ω_k^2.

Residual error was modeled by assuming:

$$y_{ij} = \hat{y}_{ij} + \varepsilon_{ij} \qquad \text{(MRS)}, \tag{6}$$

$$y_{ij} = \hat{y}_{ij} + \frac{\varepsilon_{ij} \cdot V_{max}}{S_0} \qquad \text{(MRS)}, \tag{7}$$

where y_{ij} is the observation in individual i at time j, $\hat{y}_{ij}$ is the corresponding model prediction as derived from the individual parameters P_{ki} (Eq. 5), and ε varies randomly with mean zero and variance σ^2. ε was scaled by V_{max}/S_0 for the MRI measurements to take into account the different magnitudes of the volume measurements (up to 1.5 ml) and the FLAMP-reference signal intensity ratios (up to 0.3).

The initial FLAMP-reference signal intensity ratio in each individual, $S_{0,i}$, was assumed to differ randomly from the first individual measurement, y_{i1}, whereby the variance of these differences across individuals is equal to the overall residual variance, σ^2. (This procedure saves the estimation of two extra population parameters, a mean S_0 (which is not really of interest) and an extra interindividual variance of S_0 [26, 28].)

The inter-individual variances of t_{lag}, λ, and V_{max} were estimated to be close to zero and could then be fixed to zero without a significant change in the goodness of fit or the remaining parameter estimates.

After fitting a mixed-effects model, individual parameter estimates can be obtained as maximum a-posteriori probability (MAP) Bayesian estimates for those parameters where non-zero interindividual variances have been estimated. Such individual MAP Bayesian estimates were obtained for V_{min}, fr, and S_0, and were used along with the population means of V_{max}, t_{lag}, and λ to calculate the model prediction curves for animals 1–3 (Fig. 5).

The data of animal no. 4 were analyzed individually (with the model of Eqs. 1, 2, 3, 4, 6, 7), because its kinetics obviously differed qualitatively from those of the other animals, as did the shape of the drug depot (cf. Fig. 4 vs. Fig. 3).

The program package NONMEM [1] was used for mixed-effects and individual kinetic modeling, and R [31] was used for graphical and other statistical analyses. The goodness of fit of competing kinetic models with different numbers of parameters was compared by applying the likelihood-ratio test with $\alpha < 0.05$ [40].

Results

All in vivo ^{19}F MR spectra obtained during the 6 weeks observation period showed FLAMP signals ($\delta = 22.9$ ppm) with an initially high signal-to-noise ratio (SNR) (Figs. 1, 2). (The SNR of the FLAMP resonance in Fig. 1 is about 20.) TFA formed from isoflurane ($\delta = -5.0, -10.7, -11.7$ ppm) was detectable in 9 out of 25 spectra in animal nos. 2–4, with relative signal intensity (TFA/NaF reference) ranging up to 0.015.

The in vivo ^{19}F MR spectra of all examination days in animal no. 3 are shown in Fig. 2 along with transversal ^{1}H MR images of central sections of the drug depot. The distortion of the FLAMP peak at 0.7 h may be due to the inhomogenous structure of the depot as seen in the corresponding MR image. Spectral findings were consistent in animal nos. 1–3: The amount of FLAMP remained essentially unchanged during the first week and then decreased exponentially to zero (animal no. 1) or to a residual fraction of about 10% (animal no. 2) or 30% (animal no. 3) (Fig. 5, rows 1–3). Drug kinetics were different in animal no. 4 where the depot had been injected further back near the root of the tail. About 60% of the amount injected was seemingly eliminated during the first week. The FLAMP resonance peak observed after 8 days was split and had a full width at half of maximum peak height (FWHM) of 1.8 ppm (corresponding to ca. 108 Hz at 1.5 T), as opposed to 1.2 ppm (ca. 72 Hz) or less in all other spectra. The residual fraction in this animal was about 20% (Fig. 5, bottom row).

MR images showed distinct voids in the drug depot on day 1 in animal nos. 2–4 (Fig. 2, left column, first image; Fig. 3, top row; Fig. 4, top row) (no image acquired in animal no. 1 on day 1). Voids were most clearly seen in rotating 3D projections and were not observed at later times. A histologic section of a drug depot which was injected in animal no. 3 in the left flank after the last MR examination and was excised three hours later showed large regions consisting of necrotic material within the depot.

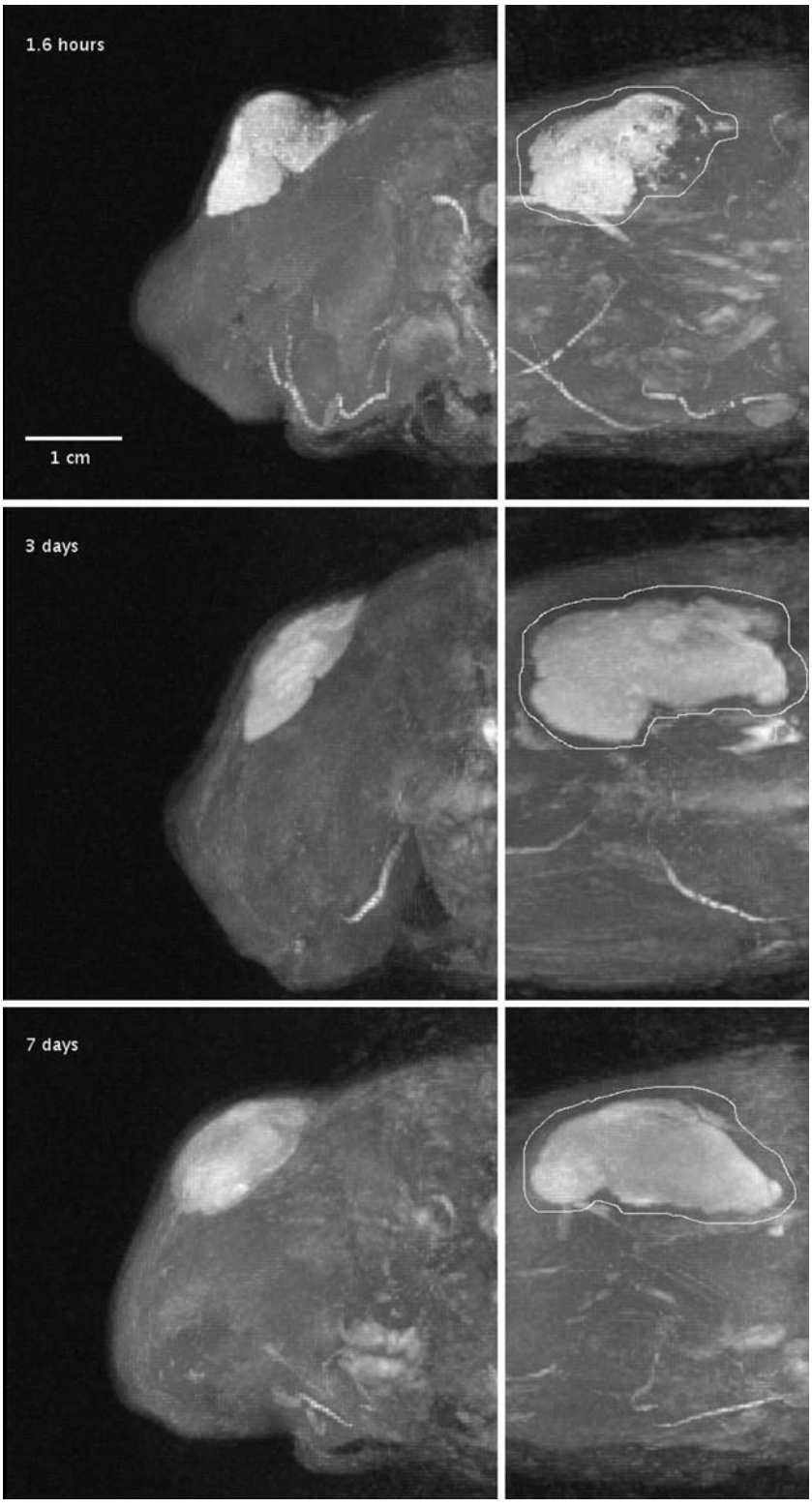

Fig. 3 Three-dimensional projections calculated from 90 transversal slices (slice thickness 0.4 mm) obtained by T_{1w} FLASH MRI (animal no. 3). Measurement parameters: see Fig. 2. *Left* axial view, in cranial to caudal direction. *Right* lateral view, from the right; delineation of drug depot derived by inspection of rotating 360° projections

The volume of the depot, as indicated by contrast enhancement, was 0.5–0.8 ml on day 1 (animal nos. 2–4) and then increased to reach values over 1 ml in all animals within the first two weeks (Fig. 5, left column, open squares). 3D projections of the depots in animal nos. 1–3 showed that they were shaped like hollow ''caps'' on day 1, becoming larger and more homogenous by day 4 (animals 2, 3), and swelling further to acquire the shape of an ellipsoid after about one week (animal nos. 1, 3) (Fig. 2, 3). The depot then shrank rapidly for two weeks (animal nos. 1–3) and thereafter remained mostly unchanged (animal no. 3, Fig. 2), or kept shrinking until

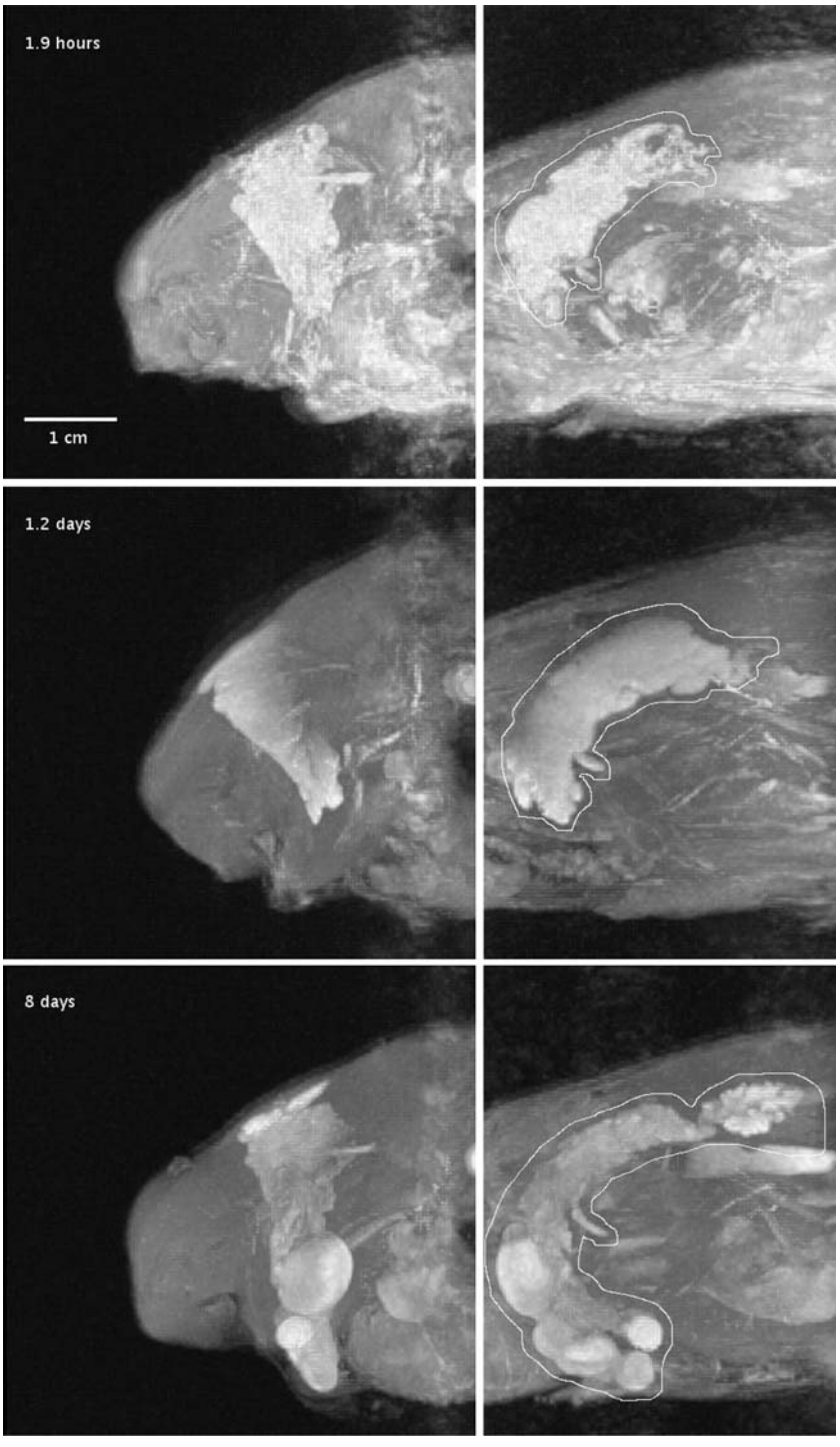

Fig. 4 Three-dimensional projections calculated from 120 (*top row*) or 110 transversal slices (*middle* and *bottom rows*) (slice thickness 0.4 mm) obtained by T_{1w} FLASH MRI (animal no. 4). Measurement parameters: see Fig. 2 (*upper row* no fat suppression). *Left* axial view, from cranial to caudal. *Right* lateral view, from the right; delineation of drug depot derived by inspection of rotating 360° projections

the end of the observation period (animal nos. 1, 2) (Fig. 5).

The shape of the drug depot developed quite differently in animal no. 4 where it had been injected further back between the hip and the origin of the tail in order to reduce the risk of motion artefacts owing to breathing. It had similar voids as the other depots on day 1, but was flatter and stretched over a larger area down towards the ventral side (Fig. 4, top row). Voids were no longer present after 1.2 days (Fig. 4, middle row). The depot then expanded on both ends in cranial direction, splitting up in five hyperintense subdepots connected by less intensely contrasted material (Fig. 4, bottom row). The release of liposome contents varied considerably within this depot in that the dorsal arm dissolved completely while the ventral arm turned into a stable remainder fraction (Fig. 5).

The results of mixed-effects modeling of FLAMP-reference signal intensity ratio and depot volume versus time in animal nos. 1–3 are given in Table 1, columns 2,

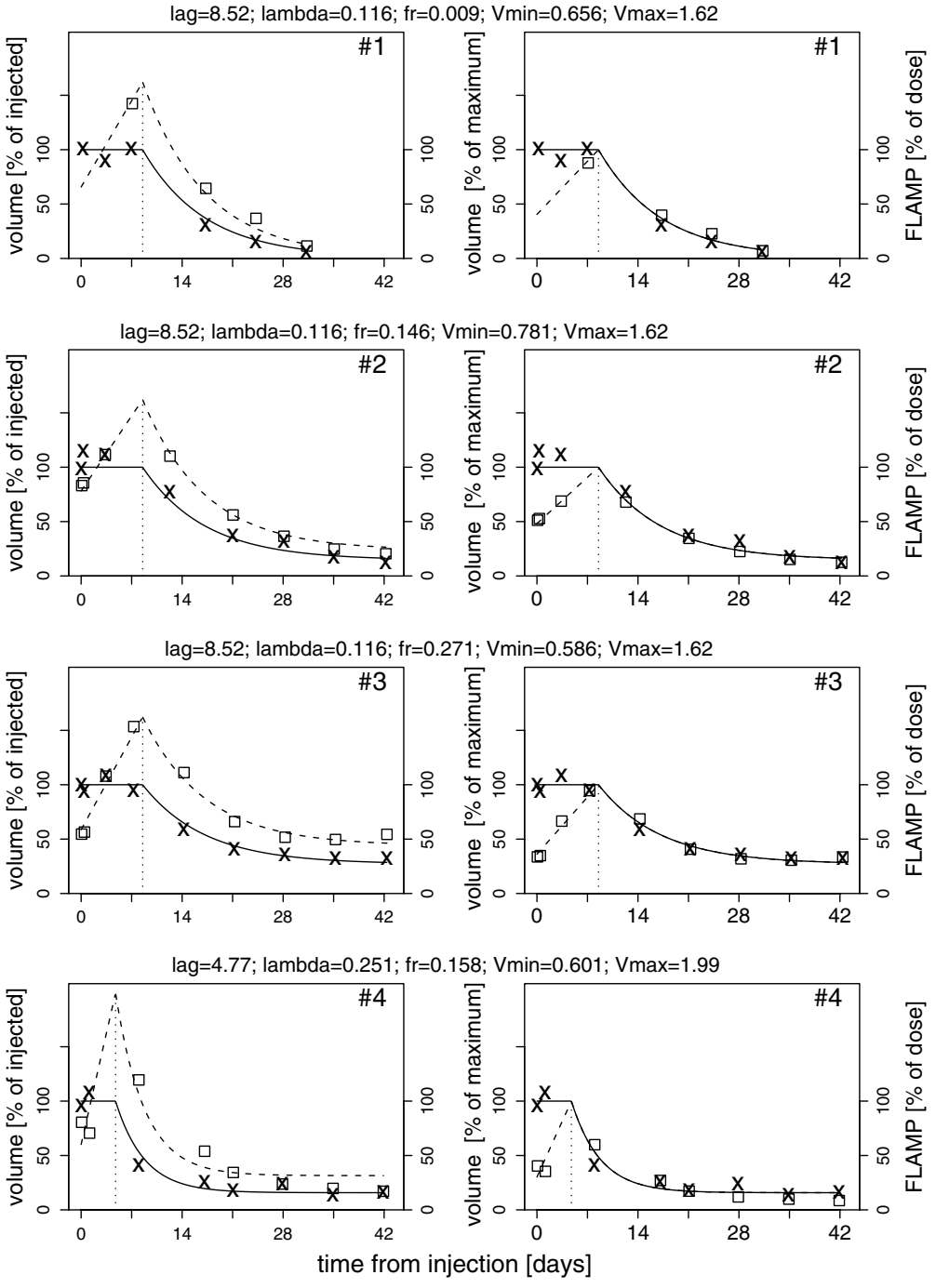

Fig. 5 Depot volume (*open squares, left ordinate*) and amount of FLAMP remaining (*cross symbols, right ordinate*) versus time after injection (animal nos. 1–4). *Solid* and *dotted curves* predicted volume and drug amount, as derived from the parameter estimates given on top of each pair of plots. Amounts calculated by setting the model-predicted initial FLAMP-reference signal intensity ratio equal to 100% of dose. *Left column* volume plotted as % of injected volume (1 ml). *Right column* volume plotted as % of maximum volume (at the end of lag time)

3, and are graphically shown in Fig. 5, rows 1–3. The estimated mean kinetic parameters (Table 1, column 2) indicate that the volume of the contrast-enhanced liposome depot increased from a (fictitious) minimum, V_{min}, of about 70% of the injected volume (1 ml) at time zero to a maximum, V_{max}, of about 160% by the end of lag time at 8.5 days. The amount of drug at the injection site and the contrast-enhanced volume then decreased with an estimated half-life of 6.0 days toward zero (animal no. 1), or toward a plateau representing a minor fraction of drug dose and maximum volume which was apparently unaffected by elimination. The individual Bayesian

Table 1 Kinetic parameters of drug release and depot volume changes

	Animal nos. 1–3; mixed-effects model		Animal no. 4, individual fit
	Mean	Inter-individual c.v.[a]	
V_{min} (ml)	0.675	17%	0.601
V_{max} (ml)	1.62	–-	1.99
t_{lag} (days)	8.52	–-	4.77
λ (1/days)	0.116	–-	0.251
fr	0.142	77%	0.158
Residual SD[b]	0.012	–-	0.015

[a]Coefficient of variation (square root of variance/population mean)
[b]Residual standard deviation of MRS data (residual standard deviation of MRI data = SD(MRS)·V_{max}/S_0)

estimates of this fraction were 0, 9, and 27% for animals nos. 1, 2, and 3, respectively.

The interindividual variances of V_{max}, t_{lag}, and λ were estimated close to zero and could be fixed to zero without a significant change in the goodness of fit or the remaining parameters. The full interindividual variance was thus not identifiable [38], and the variances of V_{max}, t_{lag}, and λ were, therefore, fixed to zero in the final model. This does not mean that they were believed to be, in fact, zero but rather that they appeared to be relatively small and could not be precisely estimated given the available data and the extent of residual variation.

The data of animal no. 4 were analyzed individually because of seemingly different kinetics (Fig. 5, bottom row). The model fit was poorer than in the other animals; the estimated parameters indicated more rapid kinetics with a shorter lag time and a shorter elimination half-life (Table 1, column 4, Fig. 5, bottom row).

The right column of Fig. 5 demonstrates that, after lag time, the time courses of the amount of FLAMP remaining (% of dose) and of the depot volume coincide if the volume is expressed as a percentage of the estimated maximum volume reached at the end of lag time.

The average ^{1}H MRI signal *intensities* of the drug depots, relative to reference tissue, stayed approximately constant throughout the observation period, irrespective of volume changes, with intra-individual coefficients of variation of 6–10%.

Estimated individual S_0 (FLAMP/reference) was 0.30 in animal no. 1 (reference: TFA 50 mM, 2 ml), and was 0.20, 0.20, and 0.22 in animals 2–4, respectively (reference: NaF 400 mM, 0.5 ml).

In a control experiment, 1 ml of a phosphate-buffered solution containing 34 µmol FLAMP and 0.21 µmol Gd-DTPA was injected subcutaneously. (The amounts of both agents corresponded to the contents of 1 ml of a liposome preparation if encapsulation efficiency is 50%.) The FLAMP-reference signal intensity ratio at 8 min after the injection was the same as S_0 in animal nos. 2–4, but dropped by more than 90% within 5 h. No FLAMP was detectable at 24 h after the injection. ^{1}H MR images (2 mm slice thickness) acquired 85 min after the injection showed a faint diffuse contrast enhancement in three adjacent layers in an area of about 12×2 mm^2 which was no longer detectable at 5.5 h after the injection.

Discussion

The results strongly suggest that simultaneous release of a hydrophilic cytostatic and a hydrophilic contrast agent from an interstitial depot may be achieved by encapsulation in multivesicular liposomes. Thus, there seems to be a potential for indirectly monitoring drug release by contrast-enhanced MRI. The data also suggest a need for individually monitoring of drug release by showing substantial variability of the extent of release between depots and even within a depot (animal no. 4).

A control experiment where FLAMP was injected as a solution showed rapid elimination of the unencapsulated drug as opposed to the slow release from liposomes. Thus, it can be assumed that the FLAMP signal in the liposome experiments contained no significant contribution from drug outside the depot region. A theoretical possibility exists that the observed reduction in ^{19}FMR signal intensity with time was merely a consequence of an efflux of Gd-DTPA resulting in an increase in ^{19}F T_1. Indeed, the ^{19}FMR signal intensity of 5-fluorouracil in rat liver in vivo has been found to be affected by the presence of Gd-DTPA [33]. In the study reported here, however, the concentration of Gd-DTPA within liposomes was seemingly constantly throughout the entire observation period, as indicated by approximately constant ^{1}H MR signal intensity, so that the observed changes of FLAMP signal intensity are likely to reflect true changes of the amount of FLAMP at the injection site.

The reason for the initial expansion of the drug depot, without a concomitant decrease in the *magnitude* of contrast enhancement, might be an influx of water between liposomes which contributes to contrast enhancement to the same extent as intra-liposomal water because of rapid exchange through the liposomal membranes [9].

The images [Figs. 3, 4 and of animal no. 2 (not shown)] and volume measurements (Fig. 5), along with the result of one histological examination, suggest that the depot is compressed during or shortly after the injection, losing water and embracing tissue fragments which soon become necrotic. The depot then keeps expanding for typically more than a week. Kinetic modeling indicates that only then the cytostatic and the contrast agent start getting released, so that it can be speculated that an influx of interstitial fluid is needed to initiate the release of liposomal contents. Events seemed to proceed more quickly in animal no. 4 (Fig. 5) where the depot split into subdepots (Fig. 4).

With the measuring procedure described, the contrast-enhanced depot volume at any instant after lag time would have to be related to the maximum volume reached at the end of lag time for an indirect assessment of the amount of cytostatic released so far. Lag time and

maximum volume would have to be estimated by fitting a kinetic model to MRI volume data obtained at regular intervals after dosing. This could be a source of uncertainty when the frequency of MRI measurements is low relative to the duration of lag time, as illustrated by the case of animal no. 4. It would, therefore, be of interest to develop a measuring procedure which excludes extraliposomal water from contributing to contrast enhancement. The contrast-enhanced depot volume might then be expected to remain constant during lag time so that the average of a few values determined during lag time could be used as a reference for assessing the extent of release of liposomal contents at later times. Such a measuring procedure might be achievable by encapsulating a shift reagent for water protons, similar to dysprosium triethylene tetramine hexaacetate (DyTTHA) which has been used in triple-quantum-filtered ^{23}Na MRS to discriminate extra- from intracellular sodium [22], and by selectively measuring the frequency-shifted protons.

The contrast agent must be rapidly eliminated from the site of the depot after release in order to be an indicator of the amount of drug remaining to be released. This was expected for Gd-DTPA at the subcutaneous administration site based on general pharmacokinetic experience [34], and was confirmed by the control experiment. The situation might be different in malignant tumors where local elimination after release could be slow and variable, such as observed for floxuridine after intratumoral injection [13, 29].

Local drug elimination after subcutaneous injection of multivesicular liposome depots has been monitored invasively in mice earlier. Monoexponential elimination without a lag time was seen for cytosine arabinoside [16], bleomycin [35], and morphine [17] while the local elimination of methotrexate was relatively slow during the first week and much more rapid during the second week after injection [3]. The local elimination of the tritium cholesterol label of multivesicular liposomes followed a similar temporal pattern as that of methotrexate [4]. Thus, it appears that the degradation of the liposomal matrix is initially delayed but not necessarily so the release of drugs.

The temporal parallelity of the release of the cytostatic and the contrast agent, despite their different molecular masses (FLAMP: 365 Da, Gd-DTPA: 550 Da) and water solubilities [FLAMP: >0.25 M (sodium salt) [2], Gd-DTPA: >1 M (dimeglumine salt) [10]], is most easy to explain by assuming that both agents are released only upon disintegration of the liposomal membranes, rather than by diffusion through intact membranes. If this is true, then Gd-DTPA could be expected to be a suitable tracer for any drug which is sufficiently large in molecular size and sufficiently hydrophilic to be retained in liposomes until disintegration of the liposomal membranes. One might consider preparing monophosphate ester prodrugs, analogous to FLAMP, of cytostatic nucleosides like gemcitabine, floxuridine, 5-fluoruridine, cytosine arabinoside, 6-methylpurine riboside, and 2-fluoroadenosine [24], in order to achieve effective retention in liposomes and trace release with Gd-DTPA. Triamcinolone acetonide phosphate is an example of a monophosphate ester pro-drug which has deliberately been prepared to achieve effective retention in liposomes.

Conclusions

The preliminary findings suggest that simultaneous release of a hydrophilic cytostatic and a hydrophilic contrast agent from a depot preparation in vivo can be achieved by encapsulation in multivesicular liposomes. Thus, there seems to be a potential for non-invasive, indirect monitoring of drug release by contrast-enhanced MRI.

Acknowledgements We are indebted to Dr. William E. Hull for preparatory in vitro MRS experiments, to Dr. Rainer Umathum for building the ^{19}F/^{1}H animal resonator, and to Dr. Volker Amelung for the pathohistological evaluation of tissue sections.

References

1. Beal SL, Sheiner LB (eds) (1999) NONMEM version V.1.1, User's guides. NONMEM Project Group, University of California San Francisco, San Francisco
2. Blumbergs P (1992). U. S. Pat. No. 5,110,919. URL: http://www.patft.uspto.gov/netahtml/srchnum.htm
3. Bonetti A, Chatelut E, Kim S (1994) An extended-release formulation of methotrexate for subcutaneous administration. Cancer Chemother Pharmacol 33:303–306
4. Brownson EA, Langston M, Tsai AG, Gillespie T, Davis TP, Intaglietta M, Sankaram MB (1998) Biodistribution during sustained release from DepoFoam(™), a lipid-based parenteral drug delivery system. Proc Int Symp Control Rel Bioact Mater 25:42–43
5. Chamberlain MC, Khatibi S, Kim JC, Howell SB, Chatelut E, Kim S (1993) Treatment of leptomeningeal metastasis with intraventricular administration of depot cytarabine (DTC 101). A phase I study. Acta Neurol 50:261–264
6. Chen HA, Le Visage C, Qiu B, Du X, Ouwerkerk R, Leong KW, Yang X (2005) MR imaging of biodegradable polymeric microparticles: a potential method of monitoring local drug delivery. Magn Reson Med 53:614–620
7. Cullis PR, Hope MJ, Bally MB, Madden TD, Mayer LD, Janoff AS (1987) Liposomes as pharmaceuticals. In: Ostro MJ (eds) Liposomes. From biophysics to therapeutics. Marcel Dekker, New York, pp 39–72
8. Domb AJ (1995) Polymeric carriers for regional drug therapy. Mol Med Today 1:134–139
9. Donahue KM, Weisskoff RM, Burstein D (1997) Water diffusion and exchange as they influence contrast enhancement. J Magn Reson Imag 7:102–110
10. Felix R, Semmler W, Schörmer W, Laniado M (1985) Kontrastmittel in der magnetischen Resonanztomographie. Fortschr Röntgenstr 142(6):641–646
11. Firth G, Oliver AS, McKeran RO (1984) Studies on the intracerebral injection of bleomycin free and entrapped within liposomes in the rat. J Neurol 47:585–589
12. Fleming AP, Saltzman WM (2002) Pharmacokinetics of the carmustine implant. Clin Pharmacokinet 41(6):403–419
13. Gandhi V, Plunkett W (2002) Cellular and clinical pharmacology of fludarabine. Clin Pharmacokin 41:93–103

14. Guerin C, Olivi A, Weingart JD, Lawson HC, Brem H (2004) Recent advances in brain tumor therapy: local intracerebral drug delivery by polymers. Inv New Drugs 22:27–37
15. Harrington KJ, Mohammadtaghi S, Uster PS, Glass D, Peters M, Vile RG, Stewart JSW (2001) Effective targeting of solid tumors in patients with locally advanced cancers by radiolabeled pegylated liposomes. Clin Cancer Res 7:243–254
16. Kim S, Howell SB (1987) Multivesicular liposomes containing cytarabine for slow-release sc administration. Cancer Treat Rep 71(5):447–450
17. Kim T, Kim J, Kim S (1993) Extended release formulation of morphine for subcutaneous administration. Cancer Chemother Pharmacol 33:187–190
18. Mantripragada S (2002) A lipid based depot (DepotFoam technology) for sustained release drug delivery. Prog Lipid Res 41:392–406
19. Mardor Y, Rahav O, Zauberman Y, Lidar Z, Ocherashvilli A, Daniels D, Yiftach R, Maier RSE, Orenstein A, Ram Z (2005) Convection-enhanced drug delivery: increased efficacy and magnetic resonance image monitoring. Cancer Res 56(15):6858–6863
20. Mayer LD, Hope MJ, Cullis PR, Janoff AS (1985) Solute distributions and trapping efficencies observed in freeze-thawed multilamellar vesicles. Biochim Biophys Acta 817:193–196
21. Menei P, Benoit JP (2003) Implantable drug-releasing biodegradable microspheres for local treatment of brain glioma. Acta Neurochir Suppl 88:51–55
22. Navon G (1993) Complete elimination of the extracellular ^{23}Na NMR signal in triple quantum filtered spectra of rat hearts in the presence of shift reagents. Magn Reson Med 30:503–506
23. Orenberg EK (2004) Intralesional chemotherapy with injectable collagen gel formulations. In: Brown DM (eds) Drug delivery systems in cancer therapy. Humana Press, Totowa, pp 229–246
24. Parker WB, Allan PW, Hassan AE, Secrist JA III, Sorscher EJ, Waud WR (2003) Antitumor activity of 2-fluoro-2′-deoxyadenosine against tumors that express *Escherichia coli* purine nucleoside phosphorylase. Cancer Gene Ther 10:23–29
25. Port R (2003) SOP 14: population pharmacokinetic analysis. In: Gastl G, Berdel W, Edler L, Jaehde U, Port R, Mross K, Scheulen M, Sindermann H, Dittrich C (eds) Standard operating procedures for clinical trials of the CESAR Central European Society for Anticancer Drug Research—EWIV. Onkologie 26(Suppl 6):60–66. URL: http://www.content.karger.com/ProdukteDB/produkte.asp?doi = 000075017
26. Port RE (1996) Estimating individual pretreatment levels of a pharmacologic response variable. Population Approach Group in Europe, Sandwich UK, June 14–15. URL: http://www.pagemeeting.org/
27. Port RE (2003) Populations-Pharmakokinetik und individuelle Dosisanpassung. In: Zeller WJ, zur Hausen H (eds) Onkologie—Grundlagen, Diagnostik, Therapie, Entwicklungen (16. Ergänzungslieferung). ecomed-Verlag, Landsberg, pp IV-8.1, 1–13 URL: http://www.dkfz-heidelberg.de/pharmakologie/04_IV-8.1_Port.pdf
28. Port RE, Ding RW, Fies T, Schaerer K (1998) Predicting the time course of haemoglobin in children treated with erythropoietin for renal anaemia. Br J Clin Pharmacol 46:461–466
29. Port RE, Hanisch F, Becker M, Bachert P, Zeller J (1999) Local disposition kinetics of floxuridine after intratumoral and subcutaneous injection as monitored by ^{19}F-nuclear magnetic resonance spectroscopy *in vivo*. Cancer Chemother Pharmacol 44:65–73
30. Port RE, Knopp MV, Brix G (2001) Dynamic contrast-enhanced MRI using Gd-DTPA: interindividual variability of the arterial input function and consequences for the assessment of kinetics in tumors. Magn Reson Med 45:1030–1038
31. R Development Core Team (2004) R: a language and environment for statistical computing. R Foundation for Statistical Computing. ISBN 3-900051-00-3. URL: http://www.R-project.org
32. Rasband W, National Institute of Mental Health, Bethesda (2004). ImageJ. Image processing and analysis in java. URL: http://www.rsb.info.nih.gov/ij/
33. Rowland IJ, Maxwell RJ, Baluch S, Ojugo ASE, Griffiths JR, Leach MO (1993) Differential distribution of 5-fluorouracil and α-fluoro-β-alanine in both rat liver and tumour. In: Proceedings of the society of magnetic resonance in medicine (SMRM), vol 1, New York, pp 244
34. Rowland M, Tozer TN (1995) Clinical pharmacokinetics: concepts and applications, 3rd edn. Williams & Wilkins, Baltimore
35. Roy R, Kim S (1991) Multivesicular liposomes containing bleomycin for subcutaneous administration. Cancer Chemother Pharmacol 28:105–108
36. Rubesova E, Berger F, Wendland MF, Hong K, Stevens KJ, Gooding CA, Lang P (2002) Gd-labeled liposomes for monitoring liposome-encapsulated chemotherapy. Acad Radiol 9(Suppl 2):S525–S527
37. Saito R, Bringas JR, McKnight TR, Wendland MF, Mamot C, Drummond DC, Kirpotin DB, Park JW, Berger MS, Bankiewicz KS (2004) Distribution of liposomes into brain and rat brain tumor models by convection-enhanced delivery monitored with magnetic resonance imaging. Cancer Res 64:2572–2579
38. Sheiner LB (1985) Analysis of pharmacokinetic data using parametric models. II. Point estimates of an individual's parameters. J Pharmacokin Biopharm 13:515–540
39. Sheiner LB, Ludden TM (1992) Population pharmacokinetics/dynamics. Annu Rev Pharmacol Toxicol 32:185–209
40. Sheiner LB, Rosenberg B, Marathe VV (1977) Estimation of population characteristics of pharmacokinetic parameters from routine clinical data. J Pharmacokin Biopharm 5:445–479
41. Viglianti BL, Abraham SA, Michelich CR, Yarmolenko PS, MacFall JR, Bally MB, Dewhirst MW (2004) In vivo monitoring of tissue pharmacokinetics of liposome/drug using MRI: illustration of targeted delivery. Magn Reson Med 51:1153–1162
42. Voges J, Reszka R, Gossmann A, Dittmar C, Richter R, Garlip G, Kracht L, Coenen HH, Sturm V, Wienhard K, Heiss WD, Jacobs AH (2002) Imaging-guided convection-enhanced delivery and gene therapy of glioblastoma. Ann Neurol 54:479–487